Published in Sedimentology 51 : 745-765, 2004,
which should be used for any reference to this work

Microbe–mineral interactions: early carbonate precipitation in a hypersaline lake (Eleuthera Island, Bahamas)

C. DUPRAZ*, P. T. VISSCHER†, L. K. BAUMGARTNER† and R. P. REID‡
*Institute of Geology, University of Neuchâtel, Rue Emile-Argand 11, 2007 Neuchâtel, Switzerland (E-mail: christophe.dupraz@unine.ch)
†Department of Marine Sciences, University of Connecticut, 1084 Shennecossett Road, Groton, CT 06340, USA
‡RSMAS – University of Miami, 4600 Rickenbacker CSWY, Miami, FL 33149, USA

ABSTRACT

Microbialites (benthic microbial carbonate deposits) were discovered in a hypersaline alkaline lake on Eleuthera Island (Bahamas). From the edge towards the centre of the lake, four main zones of precipitation could be distinguished: (1) millimetre-sized clumps of Mg-calcite on a thin microbial mat; (2) thicker and continuous carbonate crusts with columnar morphologies; (3) isolated patches of carbonate crust separated by a dark non-calcified gelatinous mat; and (4) a dark microbial mat without precipitation. In thin section, the precipitate displayed a micropeloidal structure characterized by micritic micropeloids (strong autofluorescence) surrounded by microspar and spar cement (no fluorescence). Observations using scanning electron microscopy (SEM) equipped with a cryotransfer system indicate that micrite nucleation is initiated within a polymer biofilm that embeds microbial communities. These extracellular polymeric substances (EPS) are progressively replaced with high-Mg calcite. Discontinuous EPS calcification generates a micropeloidal structure of the micrite, possibly resulting from the presence of clusters of coccoid or remnants of filamentous bacteria. At high magnification, the microstructure of the initial precipitate consists of 200–500 nm spheres. No precipitation is observed in or on the sheaths of cyanobacteria, and only a negligible amount of precipitation is directly associated with the well-organized and active filamentous cyanobacteria (in deeper layers of the mat), indicating that carbonate precipitation is not associated with CO_2 uptake during photosynthesis. Instead, the precipitation occurs at the uppermost layer of the mat, which is composed of EPS, empty filamentous bacteria and coccoids (*Gloeocapsa* spp.). Two-dimensional mapping of sulphate reduction shows high activity in close association with the carbonate precipitate at the top of the microbial mat. In combination, these findings suggest that net precipitation of calcium carbonate results from a temporal and spatial decoupling of the various microbial metabolic processes responsible for $CaCO_3$ precipitation and dissolution. Theoretically, partial degradation of EPS by aerobic heterotrophs or UV fuels sulphate-reducing activity, which increases alkalinity in microdomains, inducing $CaCO_3$ precipitation. This degradation could also be responsible for EPS decarboxylation, which eliminates Ca^{2+}-binding capacity of the EPS and releases Ca^{2+} ions that were originally bound by carboxyl groups. At the end of these processes, the EPS biofilm is calcified and exhibits a micritic micropeloidal structure. The EPS-free precipitate subsequently serves as a substrate for physico-chemical precipitation of spar cement from the alkaline water of the lake. The micropeloidal structure has an intimate mixture of

micrite and microspar comparable to microstructures of some fossil microbialites.

Keywords Bahamas, carbonates, lacustrine, microbialite, sulphate reduction.

INTRODUCTION

Microbial communities and the mineral world are dancing a 'geobiological tango' (Nealson & Ghiorse, 2001). Environmental conditions impact on the bacterial community, which in turn alters the environment through its metabolic activities. This feedback mechanism determines the characteristic mineral products of the particular system. A model system, microbial mats, has traditionally been defined as laminated organosedimentary structures, where each mat layer contains different microorganisms with distinct metabolic activities relative to oxygen and sulphide gradients (Krumbein, 1983; Van Gemerden, 1993). This view has been somewhat modified by *in situ* measurements of microbial activities, which have revealed temporal and spatial fluctuations throughout the mat profile (e.g. Visscher *et al.*, 1998, 2002). For example, sulphate-reducing bacteria (SRB) were traditionally believed to be active during the night near the mat surface where conditions are anoxic, but it was demonstrated recently that SRB activity peaks at the mat surface under oxic conditions during the day (Canfield & Des Marais, 1991; Fründ & Cohen, 1992; Visscher *et al.*, 1992a, 2000). Microbial mats are ideal model systems for assessment of energy fluxes and carbon, nitrogen and sulphur transformations because they function as semi-closed systems in which elements are cycled with great efficiency (e.g. Krumbein, 1983; Krumbein & Swart, 1983; Stal *et al.*, 1985; Canfield & Des Marais, 1993, 1994; Van Gemerden, 1993; Krumbein *et al.*, 2003).

Owing to their laminated structure, microbial mats are considered to be analogues of stromatolites (Krumbein, 1983). However, most contemporary mats are not lithifying. Furthermore, the delicate mechanisms controlling microbe–mineral interactions, particularly the role of carbonate production in microbial metabolism, are not well understood. Carbonate precipitation in microbial mats can be seen as a byproduct of microbial metabolism (Des Marais, 1997); it can also function as an energy source through proton production outside the cell membrane (McConnaughey & Whelan, 1997). Additionally, carbonate production may be a result of the production and consumption of extracellular polymeric substances (EPS).

Microbial metabolism in many benthic systems takes place inside biofilms composed of EPS, which are produced by bacteria as an extension of the cells (Costerton *et al.*, 1995). These biofilms are increasingly recognized as highly structured systems actively manipulated by microbial cells to create microenvironments (microdomains) that allow the co-existence of diverse metabolism types (Decho, 2000). EPS are important in the protection and stabilization of these microenvironments and play a key role in capturing nutrients and controlling extracellular enzyme activities (Decho, 1990, 2000; Brading *et al.*, 1995; Little *et al.*, 1997). Channels within the EPS biofilm allow rapid solute exchange, including nutrient import and elimination of waste products, which can support other metabolic reactions. EPS can also play a key role in facilitating or inhibiting carbonate precipitation (e.g. Trichet & Défarge, 1995) through multiple mechanisms: (1) by binding bivalent cations, thereby inhibiting carbonate precipitation; (2) by forming heterogeneous microdomains, which support different types of microbial metabolism, thereby facilitating precipitation; and (3) by serving as an energy and carbon source for heterotrophic bacteria, thereby facilitating carbonate precipitation. Hence, EPS are attributed with an important role in carbonate precipitation leading to the formation of modern marine stromatolites in the Bahamas (Reid *et al.*, 2000, 2003).

Dynamics of microbe–mineral interactions are important in carbonate production in both marine and non-marine environments. There is increasing evidence that many processes traditionally considered as purely physico-chemical, such as carbonate mud production during whiting events (Robbins & Blackwelder, 1992), particle formation such as ooids and peloids (Chafetz, 1986; Castanier *et al.*, 1989; Reitner *et al.*, 1997) and carbonate cycling in terrestrial environments

(Verrecchia *et al.*, 1995; Freytet & Verrecchia, 1998, 2002), have an organic and/or biological origin. Microbially induced carbonate precipitation was crucial in metazoan reef formation during geological time, stabilizing substrate (e.g. Hillgärtner *et al.*, 2001), filling porosity between reef-building organisms (coral, sponges; e.g. Laurenti & Montaggioni, 1995; Dupraz & Strasser, 1999, 2002) and, in the absence of macroscopic metazoans, building reefs from mud precipitation (mud mounds; Bosence & Bridges, 1995; Neuweiler *et al.*, 1999, 2000).

This paper presents a conceptual model of early carbonate precipitation in a Recent alkaline and hypersaline lake. Interdisciplinary, geomicrobiological approaches are used to investigate precipitation processes in order to reconstruct the formation of this carbonate deposit in space and time. The results have implications for the understanding of fossil microbialites with comparable microstructures.

MATERIALS AND METHODS

Salt Pan (76°33′ W, 25°24′ N) is a hypersaline lake of $\approx 1{\cdot}25$ km^2 situated on Eleuthera, Bahamas (Fig. 1), located along the main road 1·5 miles N of Gregory Town (Fig. 1C). The hypersaline system consists of two lakes separated by a small road (Salt Pan in the north-west and a smaller nameless pond in the south-east). Carbonate crusts were only found in Salt Pan, where the conditions are slightly alkaline (pH 9) with daily water temperature variation between 25 °C and 40 °C. The maximum water depth is ≈ 50 cm in the middle of the lake. The salinity varies regionally from 134 PSU in the shallower area (study area 1, Fig. 1C) to 83 PSU in the deeper part where the carbonate crusts are forming (study area 2, Fig. 1C).

Samples were collected along transects in Salt Pan in March 2000, June 2001 and March 2003. In order to maximize preservation of internal

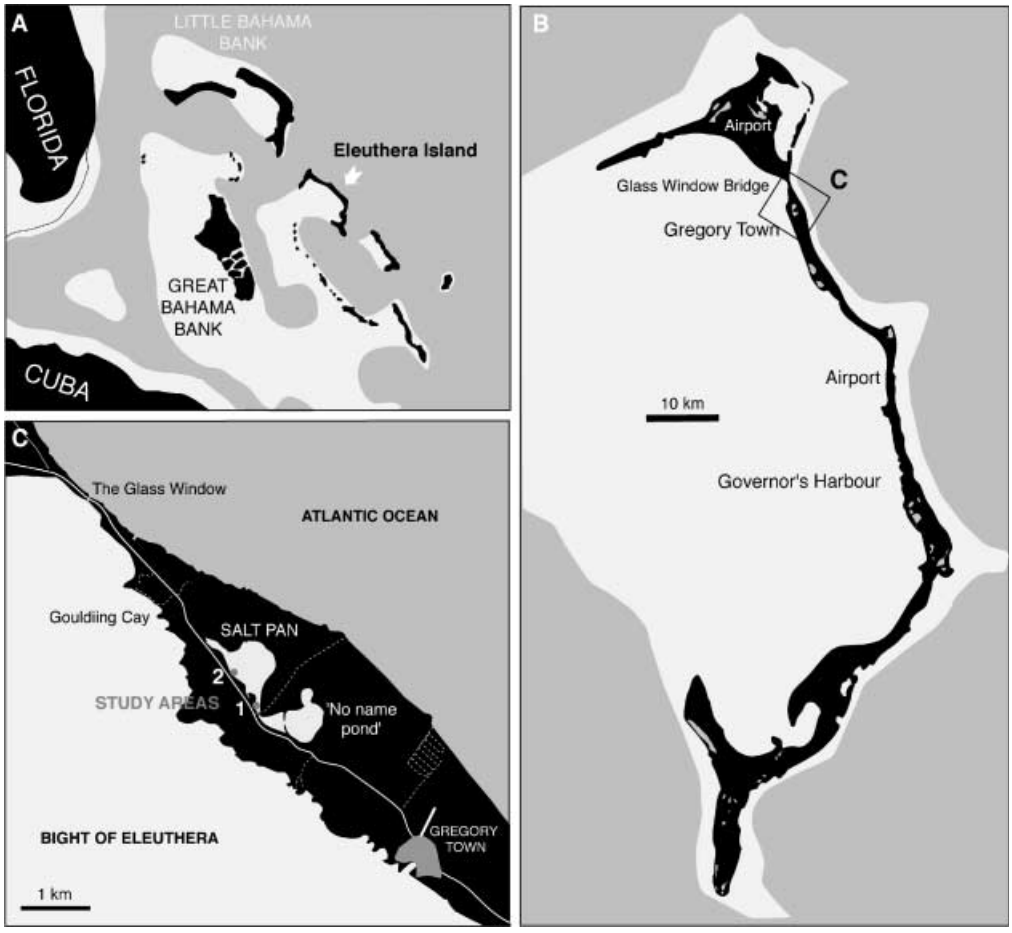

Fig. 1. Field site location. (A) The Bahamas. (B) Eleuthera Island with the location of Salt Pan. (C) Enlargement of (B) (black box) showing Salt Pan and the 'no-name' Pond, as well as the two main study areas (1 and 2).

structure, samples were fixed in a 5% solution of formalin or glutaraldehyde. Samples were kept cold and in the dark until processing. Petrographic thin sections, both 'dry' (mineral only) and 'wet' (impregnation for minerals and organic preservation), were prepared in the laboratory. Thin sections were studied using either normal light microscopy (Olympus petrographic BH-2 using Koehler illumination) or fluorescence microscopy (Olympus BX60 equipped with the following filters: excitation 395–440 nm and emission >470 nm). Colour contrast of fluorescence photomicrographs was enhanced with colour management software (Adobe PHOTOSHOP).

Fixed samples were dehydrated stepwise with ethanol (up to 100%) and dried chemically using hexamethyldisilazane (HMDS) for scanning electron microscopy (SEM). SEM analyses were conducted using a Philips XL 30 field emission environmental scanning electron microscope (FEG-ESEM), equipped with an electron backscattering pattern detector as well as an energy-dispersive X-ray spectrometer (EDS) for chemical analysis. High-vacuum observation of fixed samples was conducted in conjunction with observations of hydrated samples via the environmental control mode (wet mode). In addition, samples were frozen (cryofixation) by immersion in liquid nitrogen at −210 °C followed by sublimation under vacuum within the SEM chamber using an Oxford high-resolution cryotransfer system. This cryofixation transforms the water to ice with a crystalline domain size between 10 and 100 nm, which does not interfere with or modify the three-dimensional organization of even highly hydrated samples.

Data on the chemical composition of the various crystal textures were collected from backscattered SEM images (BSEM), EDS and X-ray diffraction (XRD) using a Scintag diffractometer. Deconvolution peaks (Pearson VII distribution functions) were used to calculate mole percentage of magnesium calcite according to the method of Kübler (1992).

Microelectrodes were used to perform field measurements of O_2 concentration in the upper 40 mm of calcified and non-calcified microbial mats. Depth profiles were determined using a rapid-responding microelectrode encased in a stainless steel needle with an outer diameter of 0·8 mm (Visscher *et al.*, 1991, 2002). Several profiles were measured in a single sample in order to assess reproducibility of the chemical gradients. Oxygen production rates were estimated using the light–dark shift method (Epping *et al.*, 1999; Visscher *et al.*, 2002): profiles were measured in the light during a quasi-steady state and then in the dark after 2, 4 and 6 min. Two-dimensional semi-quantitative distribution (mapping) of sulphate-reducing activity was carried out using silver foil coated with $^{35}SO_4^{2-}$ (Visscher *et al.*, 2000).

RESULTS

Macroscopic features

Several profiles were examined in Salt Pan on transects from the edge towards the centre of the lake. A representative profile taken in study area 2 (Fig. 1C) shows four main zones, differing in the amount and the morphology of carbonate crusts (Fig. 2). (1) Zone I is characterized by a thin microbial mat covering the muddy sediment. The top of the mat has a strongly pigmented orange colour with white millimetre-sized clumps of calcium carbonate (Fig. 3A). (2) Zone II displays a thicker and more continuous carbonate crust, still situated at the top of the mat and covered with a pigmented layer (Fig. 3B). The underlying microbial mat is also thicker, showing different coloured horizons (green, cyanobacteria; red, purple sulphur bacteria; grey to black, sulphate-reducing bacteria, as indicated by FeS/pyrite precipitate). (3) Zone III is dominated by isolated patches of carbonate precipitates with pigmented mat separated by areas of darker (FeS-containing) non-calcified microbial mat. The precipitate typically displays columnar to wall morphologies (Fig. 3C). The calcified patches are often located on small mounds resulting from sediment accumulation (Fig. 3D). Microbial mat underlying the crust is well developed and has a laminated structure (Fig. 3D). (4) Zone IV is characterized by microbial mat without precipitation (Fig. 3E and F). This thick mat colonizes the centre of the lake and shows well-developed lamination. The top of the mat is grey to black, lacking the orange pigmented layer observed in calcified mat.

Microbial composition

In every zone, the microbial mat is dominated by the filamentous cyanobacteria *Microcoleus* sp., a *Phormidium*-like form without a developed sheath, and the coccoid cyanobacteria *Gloeocapsa* sp. and *Entophysalis* sp. The uppermost layer of the mat is composed of pigments and dead material dominated by empty sheaths of

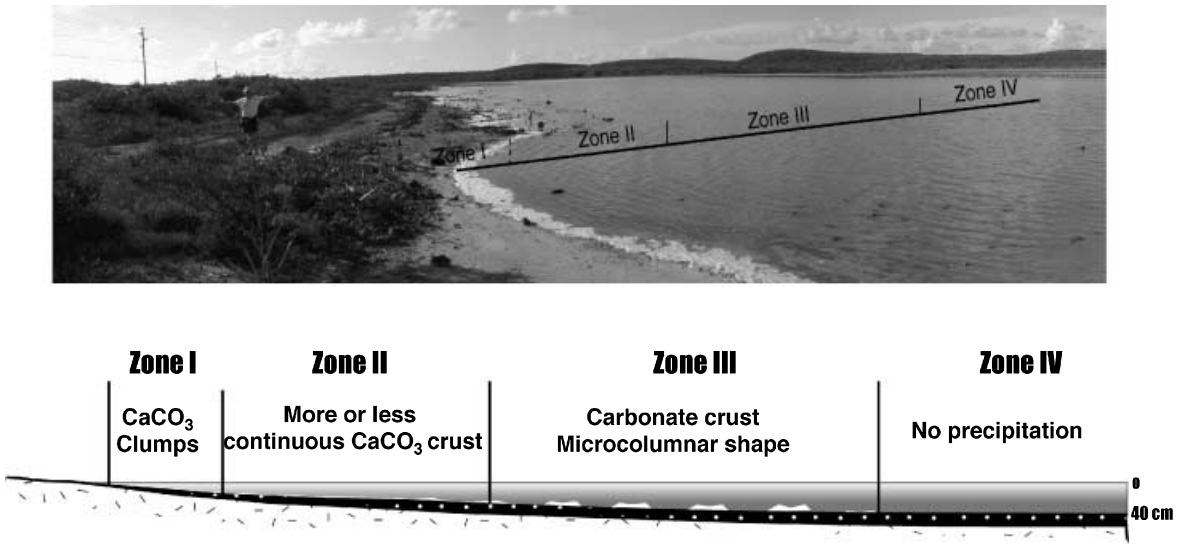

Fig. 2. Transect taken in study area 1. For zone description, see Fig. 3.

Microcoleus (Fig. 4A). The precipitation occurs in this upper layer and is covered by clusters of pigmented *Gloeocapsa* (Fig. 4D). Underneath this layer, a green mat is dominated by living *Microcoleus* (Fig. 4B) and displays numerous different bacteria, including filamentous sulphide oxidizers (Fig. 4C).

Petrographic and fluorescence microscopy

In thin section, the carbonate crust forming at the top of the mat shows a variety of microstructures (Fig. 5A and B). The base of the crust is composed of trapped sediment and is characterized by low organic content (Fig. 5C). This sediment consists of foraminifera, carbonate grains with sharp edges and micritic aggregates forming micropeloids with fuzzy borders. The grains with distinct boundaries are interpreted as trapped grains of various origins, whereas the micropeloids are more likely to be precipitated *in situ*, because they have properties similar to the precipitate crust at the surface of the mat (see below). The amount of 'fuzzy' micropeloids in the lower crust decreases with increasing depth. The lower and upper crust are separated by an organic layer, or biofilm, that lacks precipitation (Fig. 5B, black arrows), and the upper crust shows a dense micritic microstructure within an organic matrix (Fig. 5D). At the crust–water interface, the precipitate forms small columns (Fig. 5B, E and F).

At higher magnifications, the dense micritic crust (upper crust) is seen to be composed of an intimate mixture of micrite (crystal size <4 μm) and microspar (crystal between 5 and 15 μm according to Folk, 1959). The relative contribution of microspar increases from the base to the top of the precipitate crust, with a maximum at the crust–water interface. The base of the crust has almost no microspar and displays a micritic network composed of microcrystals and bacteria-like bodies (Fig. 5G). Higher in the crust, clusters of micrite are surrounded by microspar. These clusters are organized in a network that forms larger aggregates of micrite and microspar (Fig. 6A), which in turn are surrounded by microspar with larger crystals (sparite). At the crust–water interface, columns entirely surrounded by sparite (Fig. 5E and F) are partly colonized by *Gloeocapsa* sp. (Fig. 5H).

Micrite and microspar show marked differences in autofluorescence: the micrite shows a strong autofluorescence, whereas microsparite appears dark (Fig. 6B). The tops of the columns are formed of successive continuous 'microlayers' of fluorescent micrite and non-fluorescent microspar (Fig. 6C and D) often terminated by a more or less thicker and coarser microspar to spar laminae (Fig. 5H).

Chemical and microbial activity profiles

In addition to microscopic observations, microbial activity and geochemical characteristics were determined in order to gain insight into the role of microbes in the precipitation of $CaCO_3$. Development of O_2 bubbles at the surface of the lithifying mats was observed. A microbial mat in an early stage of crust formation (Zone I, Fig. 2) and another lacking carbonate precipitation (Zone

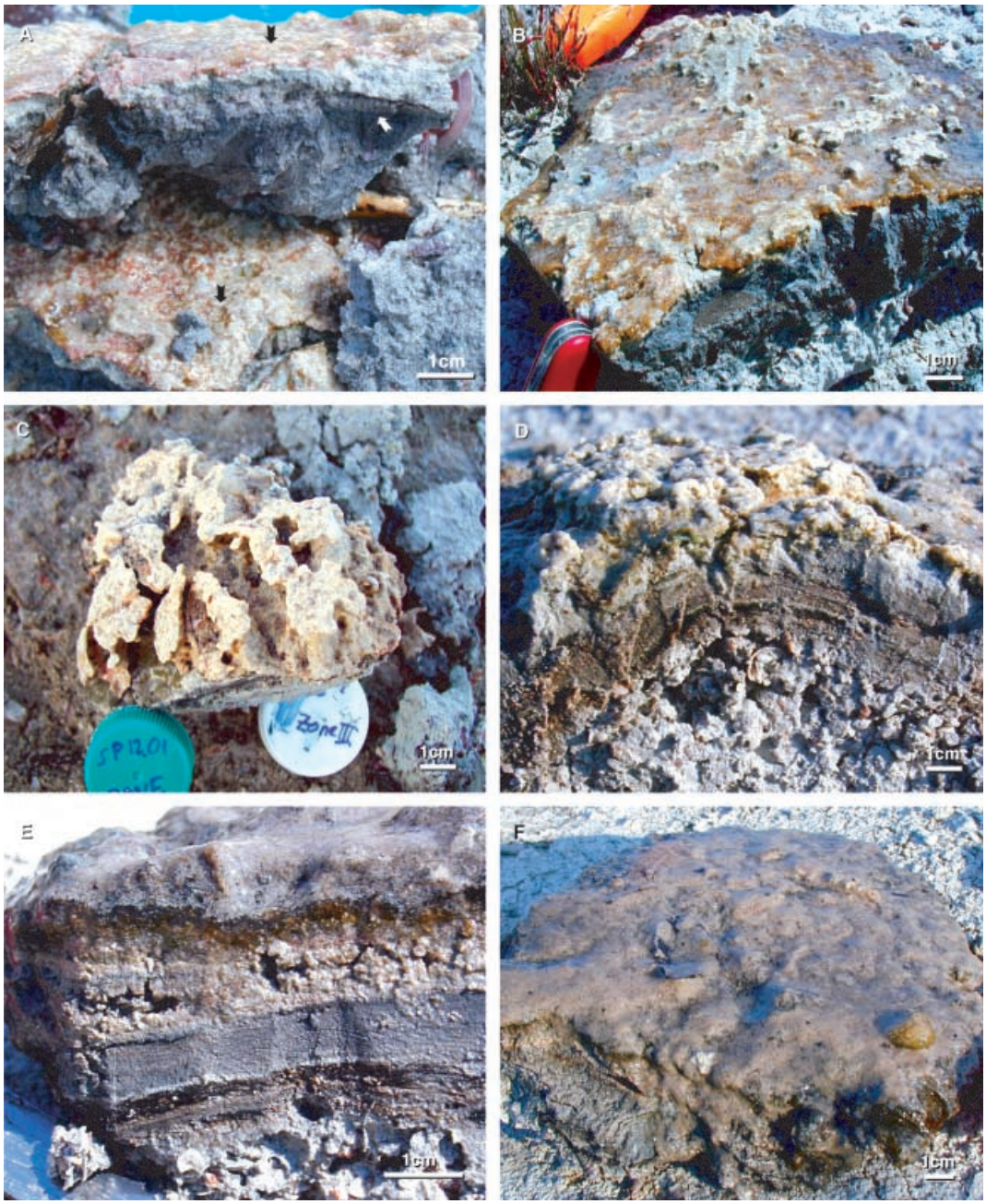

Fig. 3. Macroscopic samples from the different zones in Salt Pan. (A) Zone I displays clumps of calcium carbonate on the surface of a thin microbial mat. The mat shows a strongly pigmented top layer (black arrow). (B) Zone II presents a more continuous crust colonized in places by an orange-pigmented *Gloeocapsa* mat. (C) Zone III shows comparable crust to Zone II, but with columnar developments. (D) Zone III, patches of carbonate crust are forming on highs (relief) of underlying sediment. Note the well-developed and -laminated mat below the clotted, non-laminated carbonate deposit. (E) and (F) In the deeper part of the lake, non-calcified mat from Zone IV does not have a pigmented top layer.

IV, Fig. 2) were investigated further. Depth profiles of [O_2] revealed distinct differences between lithifying (Fig. 7C) and non-lithifying mats (Fig. 7D), although they were measured under similar light conditions (e.g. light intensities of $\approx$1950 $\mu E\ m^{-2}\ s^{-1}$). The lithifying mat displays a much steeper O_2 profile and a clear maximum of 200% O_2 saturation at 1·75 mm depth. In contrast, the profile measured in the non-lithifying mat had no clear maximum and much deeper O_2 penetration, indicating much lower O_2 production and consumption rates. This oxygen

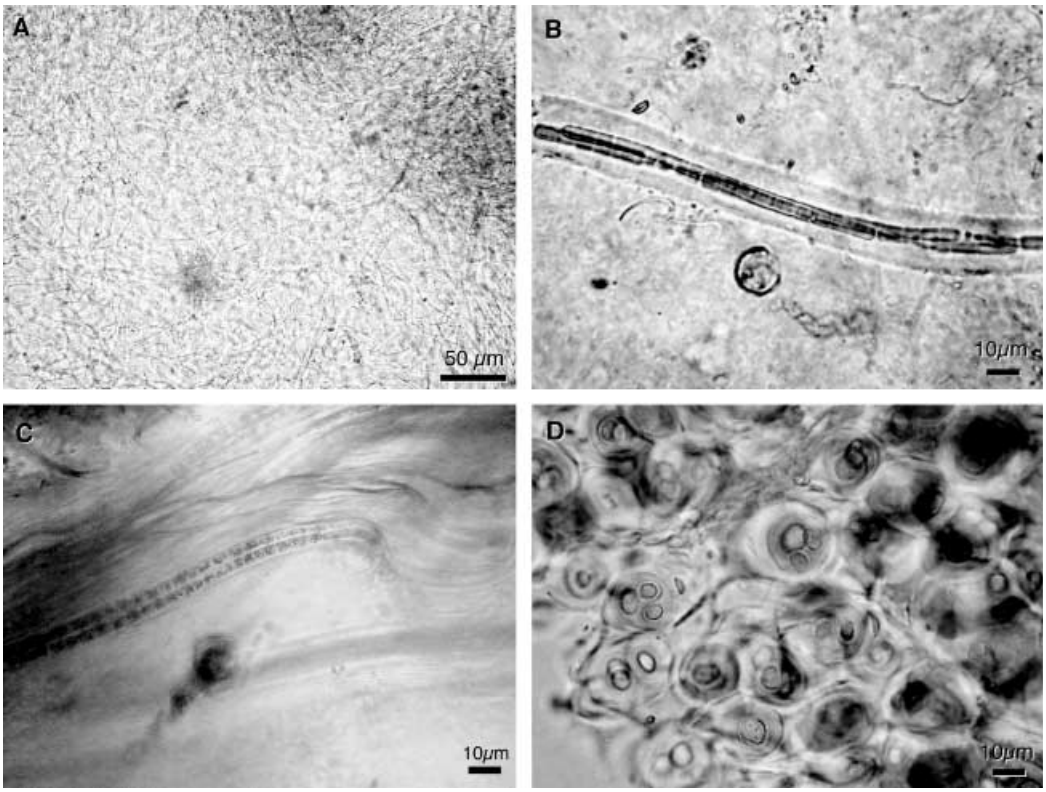

Fig. 4. Dominant organisms in microbial mats from Salt Pan. (A) Empty *Microcoleus* filaments from the top of the mat. (B) *Microcoleus* sp. taken from the green layer of the mat. (C) Filamentous sulphide oxidizers from the bottom of the green layer. Note sulphur granules inside the filament. (D) *Gloeocapsa* from the reddish-pigmented top layer covering part of the crust.

consumption results from both aerobic respiration and reoxidation of sulphide. During occasional cloud cover, the O_2 profile collapsed within seconds (especially in the lithifying mat), which indicates very high rates of O_2 consumption and that the surface of the mat encounters oxic–anoxic fluctuations throughout the day. In order to determine O_2 production as a measure of productivity, a light–dark shift experiment was performed (Epping *et al.*, 1999; Visscher *et al.*, 2002). At the depth near where the O_2 maximum was observed, the production was 74 μM O_2 min^{-1} (at 1·5 mm depth) in the lithified mat and only 5 μM O_2 min^{-1} (at 0·75 mm depth) in the soft mat.

Further evidence for different microbial activities in the lithifying and non-lithifying mats is provided by the Ag-foil data (Fig. 7A and B). Pixels indicate the presence of $Ag^{35}S$ from $^{35}SO_4^{2-}$ reduction, which represents SRB activity. Both density and individual grey tone of the pixels provide a semi-quantitative estimates of sulphate reduction rates (SRR) (Visscher *et al.*, 2000). The pixel pattern in the lithifying mat (Fig. 7A) shows an SRR peak near the surface, which corresponds with the location of the micritic crust (Fig. 3A and B). A more diffuse pixel pattern is observed below the crusty layer (Fig. 7A). In contrast, the soft mat has a dispersed pixel arrangement throughout the sample, showing no distinct area of elevated activity.

The microbial activities reported in the lithifying mat are comparable to values reported for non-lithifying mats (e.g. Canfield & Des Marais, 1991, 1994). In contrast, the non-lithifying system in Salt Pan sustained lower microbial metabolic rates.

Microstructure of the precipitate

SEM observations of frozen samples allowed investigation of the three-dimensional structure of the calcifying mat (Fig. 8). Filamentous and coccoid cyanobacteria are embedded in EPS that have a vacuolar organic network or honeycomb structure (Fig. 8A and B; e.g. Défarge *et al.*, 1996; Trichet *et al.*, 2001). The precipitation initiates inside the vacuolar structure and progressively replaces the organic network (Fig. 8C and D). High-Mg calcite fills in the space

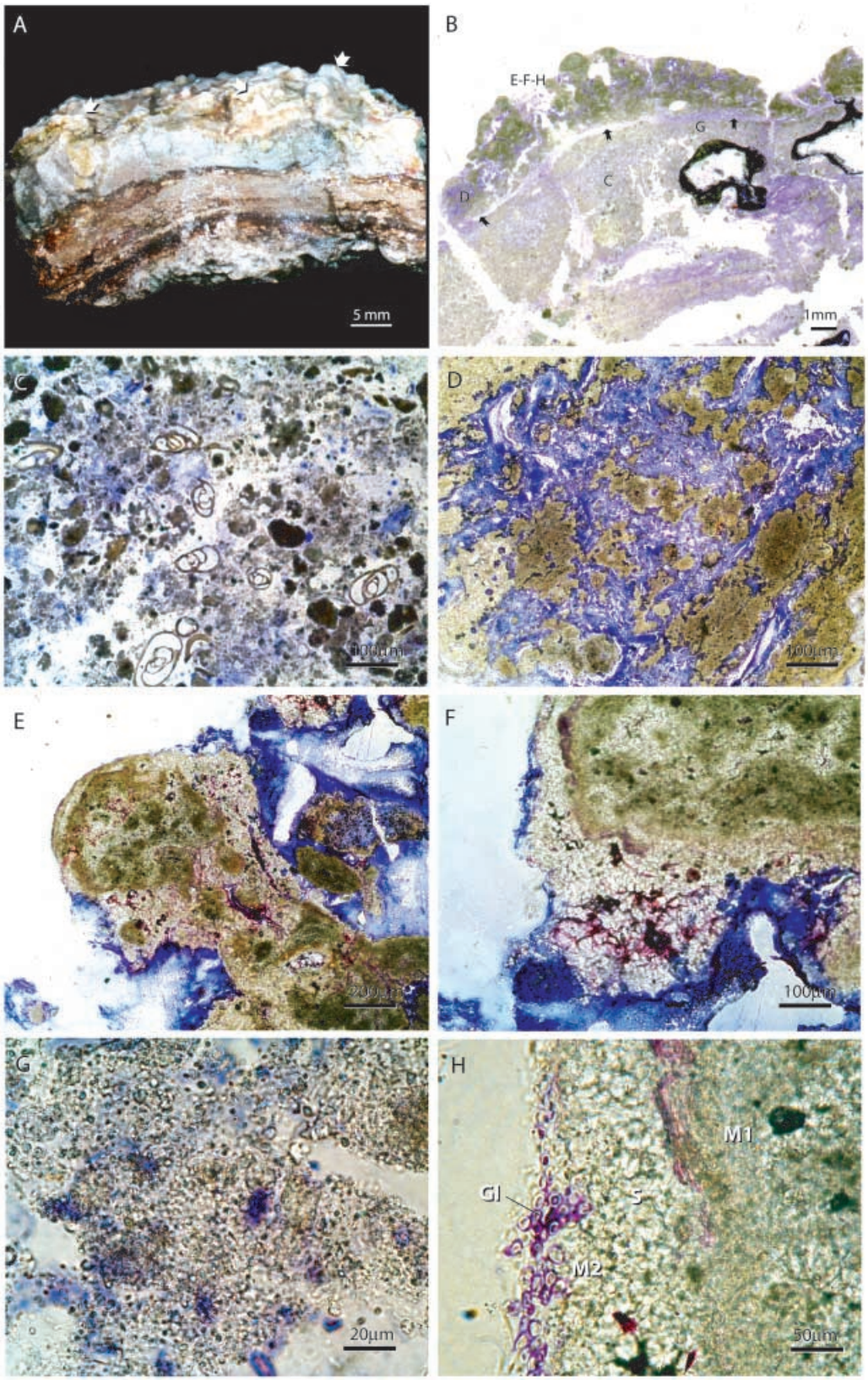

between the bacteria, sometimes resulting in bacterial 'ghosts' inside a dense calcium carbonate precipitate (Fig. 8E and F). Figure 8 presents this progressive replacement of EPS network by calcium carbonate for filamentous (Fig. 8A, C and E) and coccoid (Fig. 8B, D

Fig. 5. Microstructure of carbonate deposits found in Zone III (thin section stained with methylene blue to show organic material). (A) Typical sample showing continuous 'clotted' carbonate crust (indicated by arrows) covering well-laminated mat. (B) Overview of thin section showing different microstructures of the carbonate crust. The arrows indicate an organic layer lacking precipitation that separates the lower and upper crust. The letters refer to enlargements shown in (C) to (H). (C) Trapping and binding of carbonate particles. Grains with sharp edges are interpreted as detrital in origin, whereas micropeloids with fuzzy edges are interpreted as precipitated aggregates. Note relatively low organic content (blue colour) (D) Carbonate crust developing within an organic matrix (blue) and showing micritic microstructure. (E) Example of small column growing at crust–water interface (in the uppermost part of the crust). Note the green micrite surrounded by white microsparite and sparite. (F) Enlargement of column side presented in (E) showing microsparite inside and outside the column. Note the increase in size of spar crystals away from the column. (G) Enlargement of micritic microstructure emphasizing coccoid bacteria-like bodies (black dots) and microcrystalline high-Mg calcite (translucent crystals). (H) Detail of (F) showing microspar layer (S) overlying a micritic layer (M1) and colonized by *Gloeocapsa* (Gl) at the uppermost part of the crust. Note that another layer of micrite starts to be formed underneath the *Gloeocapsa* colony (M2). This layer is highly fluorescent (see Fig. 6).

and F) bacterial communities. No precipitation is directly associated with or found inside the sheaths of active filamentous cyanobacteria (*Microcoleus* and *Phormidium* spp.). Although very small and scattered spots of precipitation were observed in the EPS surrounding the well-oriented filamentous cyanobacteria of the photosynthetically active lower layer (Fig. 8A, see also Fig. 4), the bulk of high-Mg calcite production is associated with the top layer of the mat where the sheaths of filamentous bacteria are mostly empty or decaying and therefore no longer active (Figs 4A and 8C and E).

At higher magnification, the precipitate predominantly consists of nanometre-sized (between 200 and 500 nm in diameter) spherical bodies (Fig. 9A and B) and larger crystals (<2 μm) with smooth angular shapes (Fig. 9C). High-Mg calcite is nucleated on or has replaced the organic framework without initially breaking the three-dimensional structure of the EPS (Fig. 9A–C). In a more advanced stage of carbonate crust formation, apparently coalesced crystals mineralize most of the EPS in between bacteria (Fig. 8E and F). The precipitate is often organized in micropeloids (20–50 μm in diameter) with fuzzy edges (Fig. 9D, white arrows). The appearance of the precipitate suggests that individual aggregates of micropeloids are merging through further precipitation (Fig. 9F). The final microstructure shown in Figure 9F clearly resembles that in Figure 5D.

The mineralogy of the precipitate as determined by XRD consists of a solid solution of high-Mg calcite with 11–15 mol% Mg^{2+} substituting for Ca^{2+} (Fig. 10). Neither low-Mg calcite nor calcite was found. EDS semi-quantitative measurements on micrite and crystals indicate a very small and apparently random variation in the Mg/Ca ratio in the calcite, which indicates a stable mineralogy in the range of high-Mg calcite.

DISCUSSION

Microbial processes in Salt Pan carbonate formation

Microscopy, microelectrode observations and Ag-foil mapping reveal a clear difference in geomicrobial activity along the gradient in Salt Pan: increased lithification corresponds with increased microbial abundance and activity.

The organic matter produced by the cyanobacteria (CYN) through oxygenic photosynthesis (using light as the energy source and CO_2 as the carbon source) is oxidized by aerobic respiration (HET) using O_2 as the electron acceptor. This process consumes O_2 rapidly in the first several millimetres of the mats in Salt Pan Lake, as shown in O_2 profiles (Fig. 7C and D). Aerobic respiration leads to the formation of anoxic conditions, under which organic matter is degraded either through fermentation (FER) or by the sulphate-reducing bacteria (SRB) that use sulphate as an electron acceptor. The sulphide (H_2S) produced via sulphate-reducing activity is aerobically oxidized by the chemolithoautotrophic sulphide-oxidizing bacteria (SOB) in the oxic/anoxic transition zone. Alternatively, H_2S can also be consumed by anoxygenic photoautotrophs (e.g. purple sulphur bacteria), which typically are not the dominant sulphide oxidizers (Visscher *et al.*, 1992b). The effect of these different microbial processes can be predicted chemically in terms of net carbonate precipitation (Visscher *et al.*, 1998).

Photosynthesis (CYN):

$$2HCO_3^- + Ca^{2+} \rightarrow [CH_2O] + CaCO_3 + O_2 \quad (1)$$

Aerobic respiration (HET):

$$[CH_2O] + CaCO_3 + O_2 \rightarrow 2HCO_3^- + Ca^{2+} \quad (2a)$$

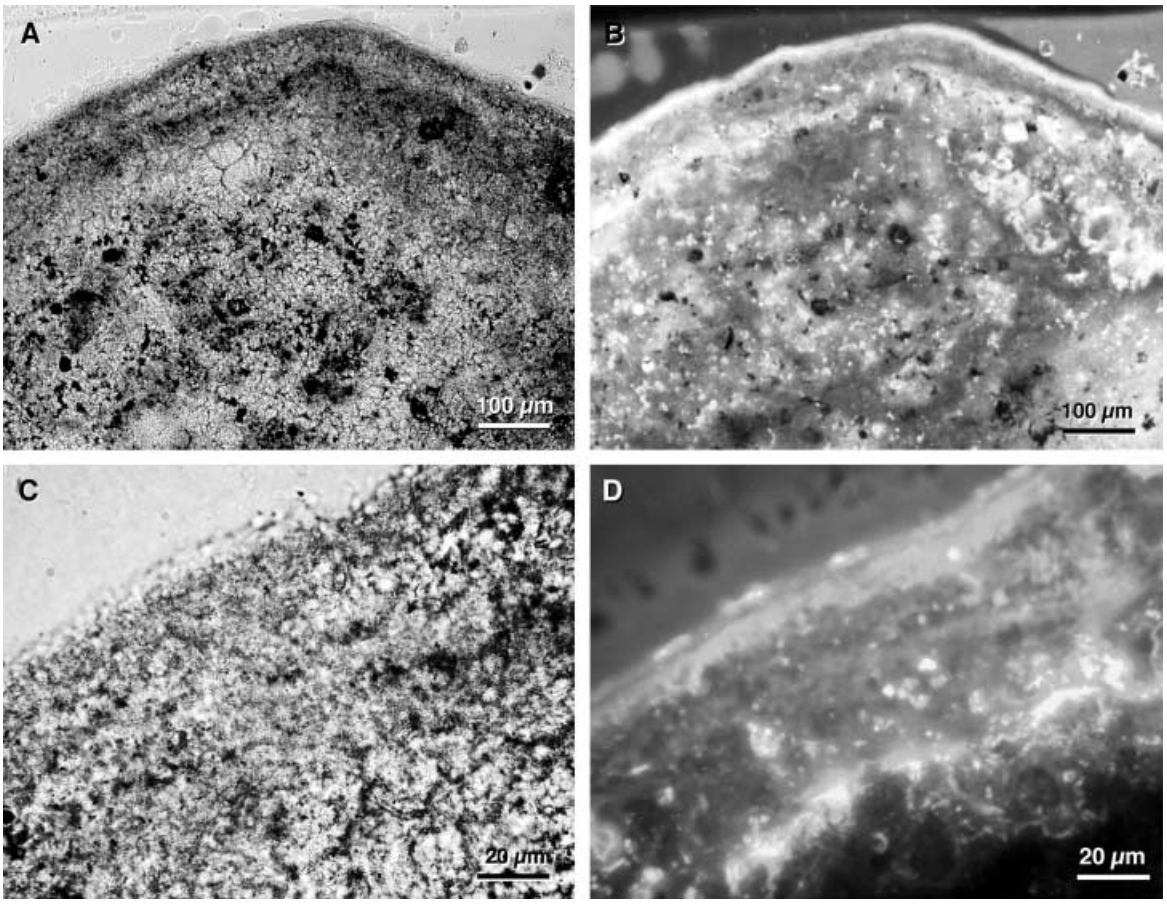

Fig. 6. Photomicrographs illustrating densely packed mixtures of micrite and microsparite in the uppermost crust. (A) Photomicrograph of the inside of a small column, showing micritic and microsparitic (to sparitic) microstructure of the precipitate. (B) Same as (A) but taken with a fluorescence microscope. Micrite shows a strong autofluorescence, whereas microsparite and sparite stay dark. Bright areas are often organized in clusters or laminae. (C) and (D) Regular light and fluorescence microscopy of the uppermost part of a small column showing successive micritic (fluorescent) and microsparitic (non-fluorescent) layers.

Fermentation (FER):

$$3[CH_2O] + CaCO_3 + H_2O \rightarrow 2HCO_3^- + Ca^{2+} + C_2H_6O \quad (2b)$$

Sulphate reduction (SRB):

$$2[CH_2O] + SO_4^{2-} + Ca^{2+} \rightarrow CaCO_3 + CO_2 + H_2O + H_2S \quad (3)$$

Sulphide oxidation (SOB):

$$H_2S + 2O_2 + CaCO_3 \rightarrow SO_4^{2-} + Ca^{2+} + H_2O + CO_2 \quad (4)$$

These simplified equations combine both biological and geochemical reactions. Equations (1) and (3) indicate that photosynthesis and sulphate reduction can result in net calcium carbonate precipitation, whereas aerobic respiration (Eq. 2a), fermentation (Eq. 2b) and sulphide oxidation (Eq. 4) result in net dissolution. The coupling of these metabolic processes is tight during the day, when copious amounts of O_2 are produced through photosynthetic activity. However, during the night, when photosynthesis ceases, rapid consumption of O_2 results in a migration of the anoxic zone towards the surface of the mat. Without oxygen and with increasing sulphide toxicity, the metabolisms of the CYN, HET and SOB slow, but some FER (depending on sulphide toxicity) and SRB remain very active, increasing the carbonate precipitation (Eqs 2b and 3). This decoupling of metabolic processes in time should result in net carbonate production, provided that the system is well buffered to absorb the CO_2 resulting from organic matter decomposition. Thus, the contribution of SRB to the total heterotrophic activity may play a decisive role in determining whether precipitation occurs (Eqs 2a, b and 3). This theory may also explain the difference in

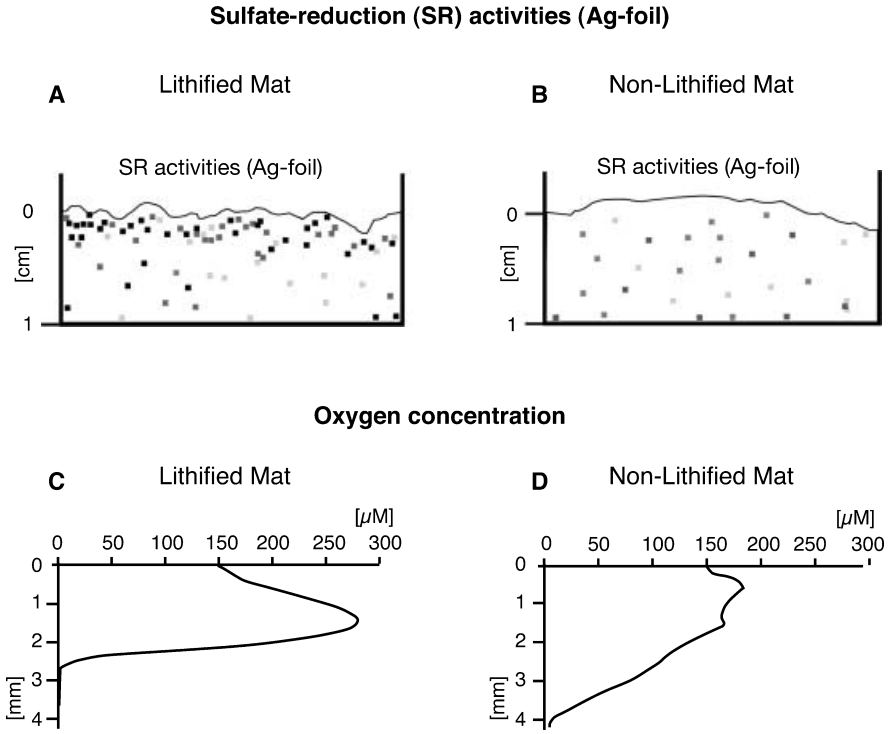

Fig. 7. Representative chemical and microbial depth profiles. Mapping of sulphate reduction bacteria activity using silver-coated foil in (A) lithified mat and (B) non-lithified mat. Both density and individual grey tone of the pixels provide a semi-quantitative estimate of sulphate reduction rates (SRR). SRB are observed in the uppermost part of the lithified mat and are associated with the carbonate crust. Representative *in situ* O_2 profiles taken in (C) lithified mat and (D) non-lithified mat.

precipitation along the transects. In contrast to the lithified mats of the outer zones of the lake, the microbial mat without precipitation (Zone IV, Fig. 2) is characterized by low microbial metabolic rates (Fig. 7) and, thus, may not form gradients that are steep enough to support the ideal spatial and temporal fluctuations and associated metabolic activities needed for carbonate production.

Carbonate precipitation was observed neither inside or on the filamentous cyanobacterial sheaths nor on the surfaces of large coccoid bacteria (*Entophysalis* and *Gloeocapsa* spp.). Additionally, very little precipitation was observed in the EPS of the lower active layer (Fig. 4). The bulk of crust formation is situated in the upper layer, where the degradation of organic material (EPS and mainly empty sheath) is largely mediated by SRB.

This observation differs from the model for calcifying cyanobacterial mats in which carbonate precipitation is caused by CO_2 uptake during cyanobacterial photosynthesis (e.g. Thompson *et al.*, 1997; Freytet & Verrecchia, 1998; Merz-Preiß & Riding, 1999). Recent studies have linked impregnation of cyanobacterial sheaths through photoautotrophic metabolism to low amounts of dissolved inorganic carbon inside the medium (Merz-Preiß & Riding, 1999; Arp *et al.*, 2001). In freshwater travertine, impregnation of filaments only occurs in slow-flowing CO_2-poor streams or lakes, whereas high-CO_2 concentration fast-flowing freshwater streams can produce $CaCO_3$-encrusted cyanobacteria through inorganic CO_2 outgassing from resurging groundwater, cascades and waterfalls (Merz-Preiß & Riding, 1999). Under alkaline conditions, microgradients created inside the cyanobacterial sheath through photoautotrophic removal of CO_2 do not play a significant role because of the large carbon pool and the strong pH buffering of the alkaline water (Arp *et al.*, 2001, 2003). In this study, neither sheath impregnation nor physicochemical incrustation of cyanobacteria was observed. Additionally, maximum activity of SRB was found in close proximity to the carbonate crust in the uppermost portion of the mat. These observations suggest a close temporal and spatial coupling of metabolic processes inside the microbial mat, with a strong role played by the SRB.

Extracellular polymeric secretion (EPS) as source of $CaCO_3$ precipitation

The relationship between EPS and carbonate precipitation is the topic of several papers (e.g.

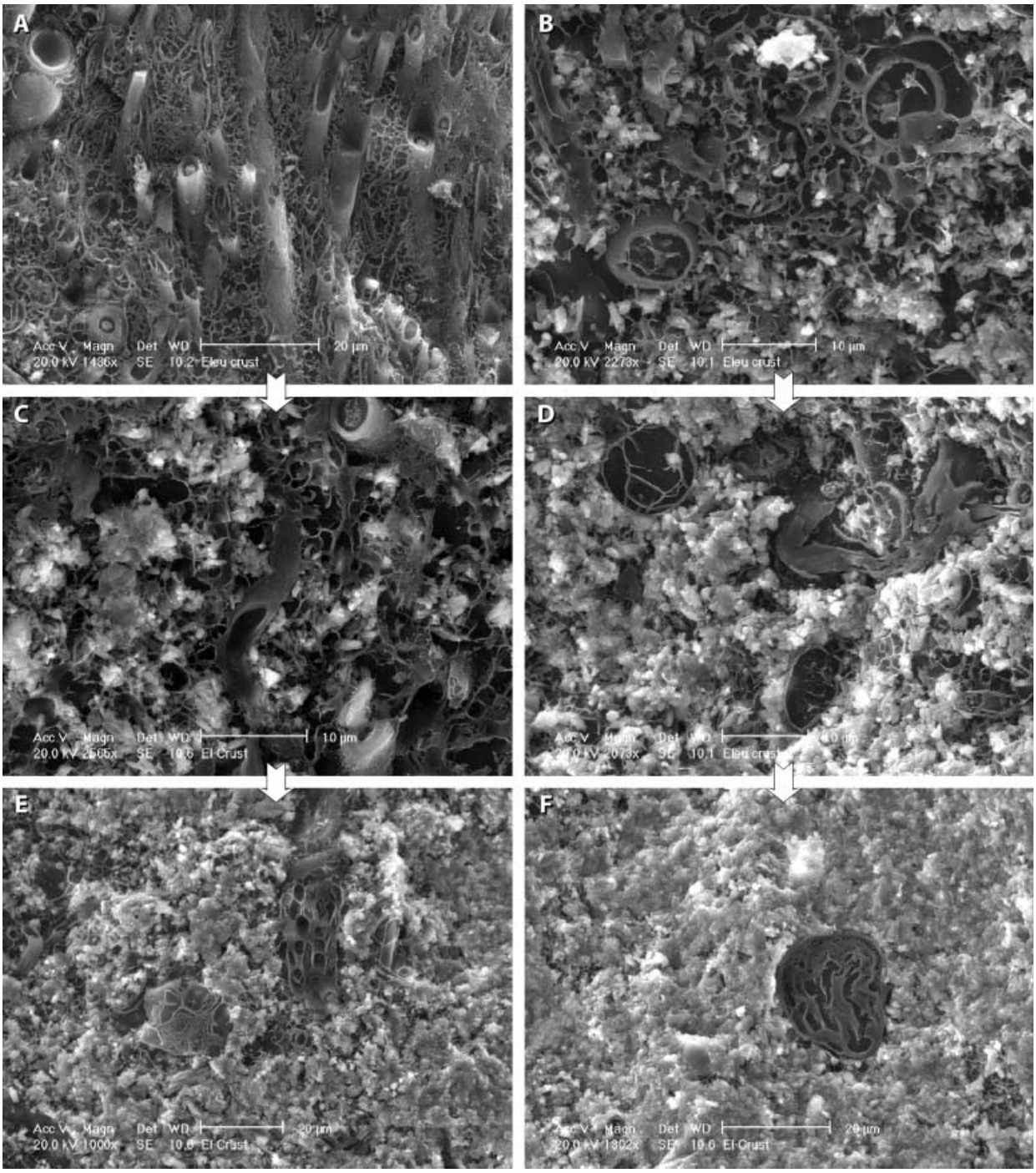

Fig. 8. Photomicrographs showing microbial communities and microstructure of precipitates as seen with FEG-ESEM using cryofixation. Sequence (A)–(C)–(E) (white arrows) represents progressive replacement of EPS alveolar structure with high-Mg calcite for filamentous-dominated community. Sequence (B)–(D)–(F) represents the same replacement for a coccoid-dominated community. (A) Well-organized filamentous cyanobacteria embedded in EPS matrix (alveolar texture) showing no significant Mg-calcite precipitation (scattered white spots inside EPS on the left). The picture is taken in the 'active' layer (green layer) below the crust. Note that most of the sheaths still show traces of trichomes. (B) Coccoid bacteria embedded in EPS. The onset of carbonate precipitation is initiated within EPS matrix. (C) and (D) EPS matrix is progressively replaced by high-Mg calcite micrite. Picture (C) shows mostly disorganized empty filaments and EPS, which is common for the top-calcifying layer of the mat. (E) and (F) EPS matrix is replaced by carbonate precipitation. Most of the filamentous cyanobacteria sheaths have disappeared, whereas some coccoids (mainly *Gloeocapsa*) are still present, completely surrounded by Mg-calcite micrite.

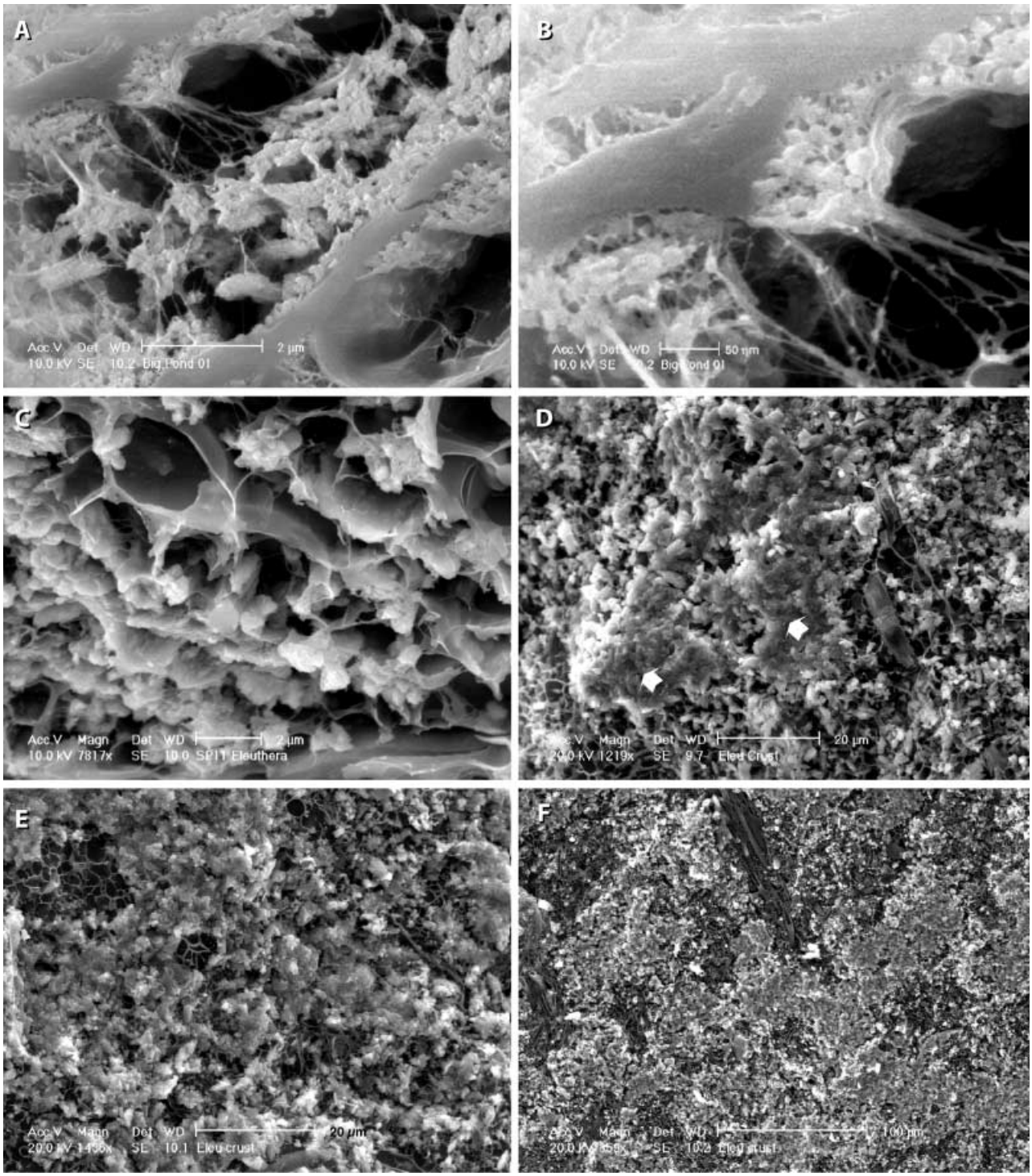

Fig. 9. ESEM detail of EPS matrix replacement by high-Mg calcite. (A) High-magnification picture showing progressive replacement of alveolar EPS walls with small Mg-calcite spheres. (B) Enlargement of the nanosphere structure of the precipitate 'feeding' on the organic structure presented in (A). (C) The nanosphere structure rapidly grows larger, smoothly angular crystals. (D) Inhomogeneous crystal coalescence in between bacteria leads to micropeloid formation (20–50 μm in diameter; white arrows). (E) and (F) Merging of individual aggregates of micropeloids resulting from continued precipitation. The result can be compared with Fig. 5D.

Pentecost, 1985; Reitner, 1993; Trichet & Défarge, 1995; Reitner *et al.*, 1995; Neuweiler *et al.*, 1999; Trichet *et al.*, 2001; Arp *et al.*, 1999a,b, 2003). Arp *et al.* (2003) presented detailed models of EPS degradation and carbonate precipitation under various environmental conditions.

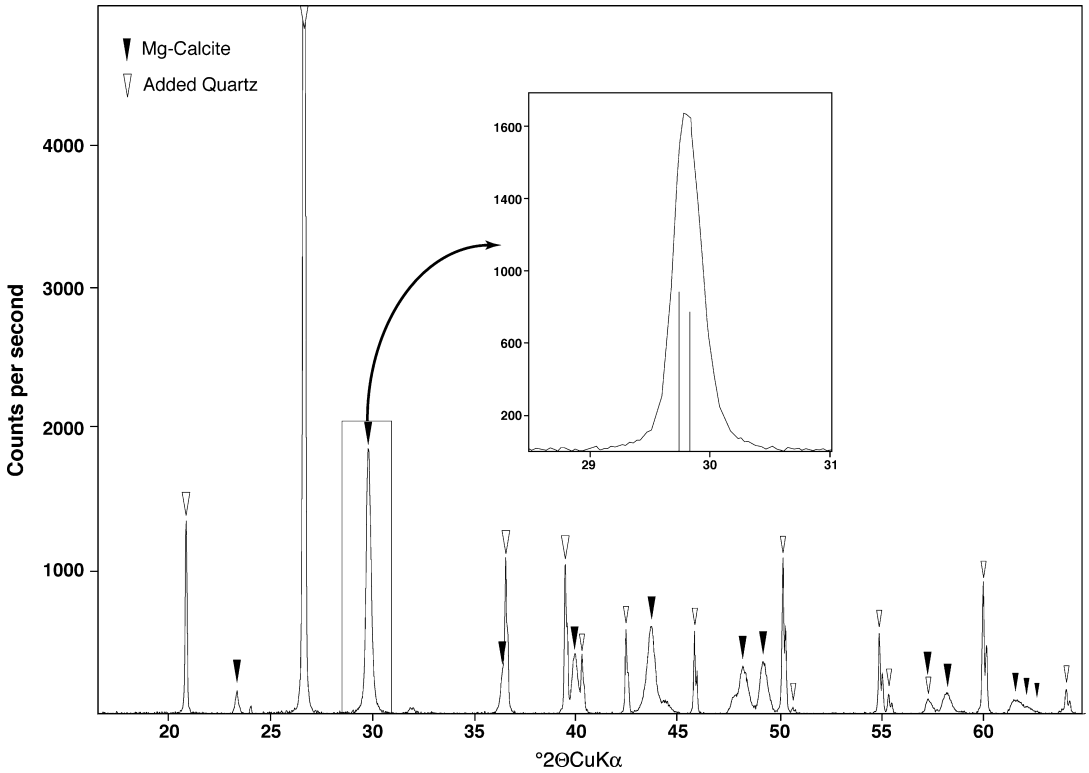

Fig. 10. X-ray diffractogram of Salt Pan microbialite. The mineralogy of the precipitate is a solid solution of high-Mg calcite with 11–15 mol% Mg^{2+} substituting for Ca^{2+}.

However, these models neglected microbial components and, notably, lacked *in situ* measurements of key metabolic processes. The present study exemplifies the importance of microbial processes with the following key findings: (1) the initial high-Mg calcite precipitation in the alveolar network of EPS that embeds filamentous and coccoid cyanobacteria (Fig. 11A, B1 and B2); and (2) a high SRB activity in close spatial relationship with the precipitated crust (Fig. 7). By combining multiple microscopic techniques and *in situ* microbial activity measurements, this study provides strong links between carbonate crust formation, EPS degradation and bacterial metabolism (particularly that of SRB).

The role of EPS in carbonate precipitation is ambiguous because of its ability to inhibit or promote calcium carbonate nucleation in specific situations. Initially, the EPS matrix acts as a 'cation sponge', inhibiting carbonate formation by removing Ca^{2+} from solution. This inhibition potential results from large amounts of macromolecules (in EPS), which contain acidic amino acids (e.g. aspartic and glutamic acids) and carboxylated polysaccharides (e.g. uronic acids), which have Ca^{2+}-binding potential (e.g. Trichet & Défarge, 1995). The Ca^{2+}-binding capacity of EPS increases with pH, because of the pH-dependent deprotonization of the carboxyl group (Ferris *et al.*, 1989). The uronic acid concentration in EPS, as well as the amount of EPS produced, increases under stress conditions in certain organisms (Uhlinger & White, 1983).

In order to allow carbonate crystal nucleation, the cation-binding capability of the EPS matrix has to be reduced. This can be achieved by (1) externally increasing ion concentration (e.g. Ca^{2+}, Mg^{2+}) in order to reach the saturation of EPS acidic bonds; (2) EPS organization into an acidic template for organomineralization (Trichet & Défarge, 1995); and (3) hydrolytic destruction of the EPS. These three mechanisms are discussed below.

External increase in cation concentration

The first mechanism is proposed for fibrous aragonite precipitation in Satonda Crater Lake, where microbialite is associated with seasonal upwelling of high-alkalinity waters followed by evaporation (Arp *et al.*, 2003). This mechanism is difficult to invoke in Salt Pan because this lake is very shallow (maximum depth 50 cm), and pH measurements at different seasons suggest that the alkalinity remains relatively constant in both deep and shallow areas. Furthermore, the upper

limit of crust formation (Fig. 2, Zone II) is below the minimum water level during the dry season, and the zone of maximum crust formation is not situated at the edge of the lake but at intermediate water depths (Fig. 2, Zone III), minimizing the effects of evaporation.

Organomineralization

In the second scenario, EPS promotes $CaCO_3$ precipitation via organomineralization (Trichet & Défarge, 1995). In mollusc shells, controlled biomineralization genetically organizes an acidic matrix, which is responsible for mineralization (e.g. Addadi & Weiner, 1989). In contrast, acidic macromolecules found in microbial biofilms are randomly distributed throughout the EPS matrix. These acidic sites have to be rearranged in an organized template to furnish efficient carbonate nucleation sites (Reitner, 1993; Trichet & Défarge, 1995). Défarge *et al.* (1996) and Trichet *et al.* (2001) proposed that decaying EPS is being reorganized into an alveolar structure (Figs 8 and 9) that could promote highly organized nucleation sites. However, in the present samples, this is unlikely to be the dominant mechanism: alveolar structure is observed across the entire microbial mat and not only in the decaying non-photosynthetically active upper part. Biomineralization cannot be ruled out completely, because a clear replacement of alveolar EPS by $CaCO_3$ is observed (Fig. 9A). However, this type of mineralization resembles the destruction and replacement of structure more than crystal growth on a reorganized organic template. Biomineralization can account for random nucleation sites observed inside the overall mat, but cannot explain the dense upper crust formation, where additional processes have to be invoked.

Increase in cation concentrations within the EPS matrix

The third process (EPS degradation) liberates large amounts of ions bound to the EPS through decarboxylation. This process increases the cation concentration in solution and, if carbonate ions are available, Mg-calcite can be produced. However, macromolecules within the EPS matrix can be very resilient and hydrolysis of EPS is not trivial. The degradation of EPS can be realized through heterotrophic metabolism (fermentation) or through destruction by UV light.

In the case of partial degradation of EPS by heterotrophic bacteria, low-molecular-weight (lmw) organic carbon is formed. This lmw organic carbon is used in sulphate reduction, which increases alkalinity and, thus, the amount of CO_3^- in solution. An internal increase in $[Ca^{2+}]$ and $[Mg^{2+}]$ through EPS hydrolysis and local augmentation of CO_3^- through sulphate reduction would promote high-Mg calcite precipitation. Under these conditions, EPS degradation by heterotrophs could theoretically enhance carbonate precipitation. Therefore, if the HET contribution to respiration (Eqs 2a and b) is outweighed by that of SRB (Eq. 3), net precipitation of carbonate occurs. If aerobic respiration outweighs sulphate reduction, dissolution of carbonate results. Interestingly, when EPS was added as the sole carbon source for respiration in laboratory experiments, it sustained higher initial rates of sulphate reduction than aerobic respiration (Visscher *et al.*, 1998, 2000, 2002). Activity of SRB was immediately enhanced upon the addition of *Schizothrix*-derived EPS, whereas HET showed a significant lag time in consumption rates after EPS was added. This difference can be explained by rapid fermentation of refractory organic matter in an anaerobic environment and release of lmw organic compounds (acetate, lactate and ethanol) fuelling SRB activity (Visscher *et al.*, 1998). While a direct association between bacterial cells and calcifying EPS was not observed, this could be explained by the production of bacterial exoenzymes. These exoenzymes would degrade the EPS without the physical involvement of the cell.

Gleocapsin, which is produced by the cyanobacterium *Gloeocapsa* sp., may be particularly important to calcification. Crust formation ceases as soon as the mat lacks a gleocapsin-containing upper layer, which occurs in the deeper part of the lake (Zone IV), inducing possible 'bathymetrical' control on carbonate precipitation. Also, in the shallow part of the lake, UV light could be strong enough to contribute to EPS decarboxylation and, thus, indirectly to carbonate production. In the deeper part of the lake, increasing depth of turbid water completely absorbs UV light, preventing decarboxylation. Decarboxylation produces CO_2 that partly diffuses into the water column, where the buffering capacity of the alkaline water of Salt Pan (pH 9) prevents an increase in pCO_2 and carbonate dissolution, similar to scenarios proposed for other systems (Arp *et al.*, 1998, 1999a,b).

Nanosphere formation and potential bacterial entombment

In the initial stage, carbonate precipitates produced by the EPS matrix are composed of

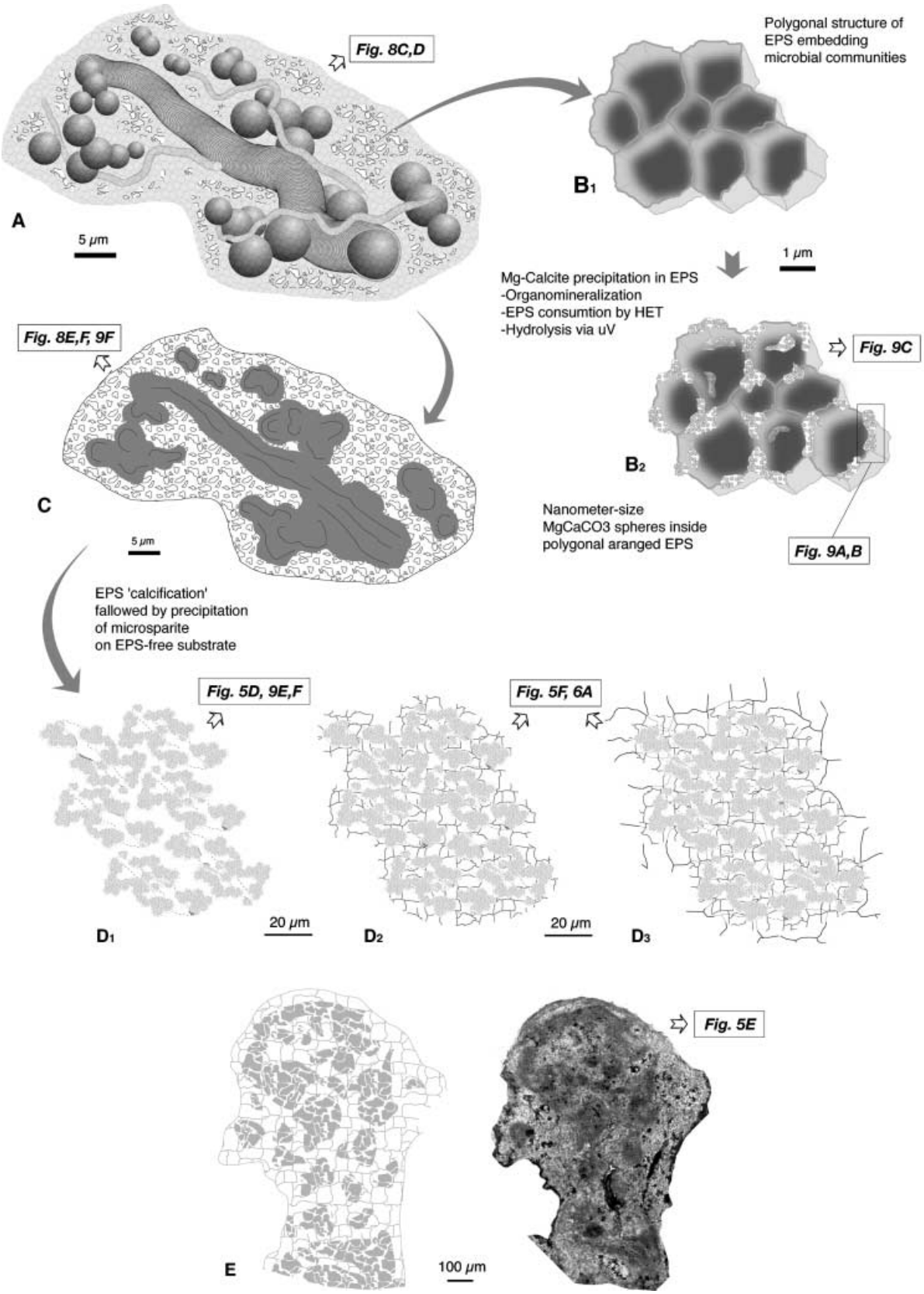

Fig. 11. Model of early carbonatogenesis in hypersaline and alkaline lake. See text for explanation.

200–500 nm spheres of Mg-calcite (Fig. 11B2). These spheres rapidly develop rounded crystal shapes and could represent a special carbonate morphology ('nanospherulite'), which forms before a more conventional crystallographic habit is developed. Experiments performed under sterile conditions with dissolved organic carbon indicate that calcite can produce euhedral crystals 50–800 nm in diameter and smaller (<50 nm) anhedral, rounded particles or protocrystals (Kirkland *et al.*, 1999). Other experiments on tissue decay have produced abundant proteinaceous spheroids that, after mineralization, can contribute to nanospherulite formation (Schieber & Arnott, 2003). According to Braissant *et al.* (2003), the composition of calcifying EPS can control $CaCO_3$ mineralogy (calcite, vaterite) and crystal morphology (spherolites, rhombs). More acidic EPS promotes spherical morphologies, which could explain the initial spherical shape of the crystal seed ('nanospherulites') observed in Salt Pan microbialite.

However, the size of these crystals is in the range of the minimum theoretical body size for active cells (200 nm; Nealson & Stahl, 1997; see also review by Knoll, 1999) and could therefore represent entombed bacteria. The entombment can be either passive or active. Passive entombment, which occurs during rapid carbonate precipitation with bacterial growth on crystal faces, was not observed in Salt Pond. During active entombment, as documented by Van Lith (2001) and Van Lith *et al.* (2003), bacterial cells adsorb bivalent cations such as Mg^{2+} and Ca^{2+}. These cations then bind with bicarbonate produced during microbial respiration, leading to mineral precipitation at the surface of the membrane. Bacteria may benefit from the cell surface calcification, because calcium precipitation induces the production of protons that generate ATP. In addition, protons can be discharged into ambient waters, locally converting HCO_3^- to CO_2, which may stimulate oxygenic photosynthesis (McConnaughey & Whelan, 1997). Finally, minerals outside the cell wall could act as catalysts, minimizing the internal enzymes required for basic metabolism and thereby decreasing cell size (Olavi Kajander *et al.*, 1999). Although Figure 9A shows structures that could be interpreted as small calcifying bacteria 'feeding' on EPS, further investigation such as cryo-transmission electron microscopy (TEM) or DNA extraction must be performed in order to validate this hypothesis.

Precipitate microstructures

Micrite to spar cement

Based on observations made in this study, a simple model for microbial deposition of calcium carbonate in the hypersaline lakes of Eleuthera was constructed (Fig. 11). The replacement of the organic matter by the mineral product occurs in sequence, from micrite to microsparite to spar cement (Fig. 11). Initially, 'nanospherulite' precipitation and/or active entombment of small bacteria results in a complete calcification of the EPS matrix that surrounds the bacteria (Fig. 11A–C). This precipitation forms micrite with a high degree of autofluorescence resulting from intracrystalline organic matter. The consumption of EPS during calcification then leads to the formation of micropeloids, which do not fluoresce. At this point, the alkaline water of Salt Pan favours spontaneous physico-chemical precipitation, which was previously inhibited by the EPS biofilm. The precipitation of microspar cement follows two steps: (1) fuzzy-edged micropeloids form between the micritic clusters (Fig. 11D1 and D2); and (2) subsequently, larger spar cement forms around the micropeloids themselves (Fig. 11D3). The final result forms patches of micropeloidal micrite with fuzzy edges surrounded by spar cement visible in thin sections (Fig. 11E). Physico-chemical precipitation from the alkaline water is also suggested by increase in microspar content (and the presence of spar cement) close to the water–crust interface (Fig. 11E).

Comparison with microstructure of fossil microbialite

Microbially induced micrite precipitation surrounded by spar cement has been described in Pleistocene travertine (Folk & Chafetz, 2000). This micropeloidal structure can also be compared with that observed in thrombolite (Aitken, 1967) in Oxfordian Jurassic Reefs (Fig. 12; Dupraz & Strasser, 1999, 2002). The mesostructure of these Jurassic thrombolites is composed of polymorphic mm- to cm-sized objects called mesoclots (e.g. Shapiro, 2000), which generally display a micropeloidal structure (Fig. 12). Although Early Palaeozoic mesoclot microstructures can clearly be related to specific calcified bacteria such as *Angusticellularia* and *Renalcis* (Riding, 2000), these micropeloids with fuzzy edges surrounded by microspar and spar cements are often merely interpreted as microbially induced structures (e.g. Kennard & James,

1986; Riding, 1991, 2002; Leinfelder *et al.*, 1996; Dupraz & Strasser, 1999). Although environmental conditions are different, precipitation in the EPS matrix of Salt Pan produces a comparable microstructure. This study provides additional evidence for the microbial origin of such fossil micropeloidal carbonate.

CONCLUSIONS

The conceptual model of early carbonate precipitation in Salt Pan includes the following processes (asterisks mark interpreted, as opposed to observed, features):

1 Precipitation is situated in the uppermost layer, which is composed of predominantly empty filamentous sheaths, coccoids and EPS. SRB activity is also highest in this carbonate crust.
2 No precipitation occurs in or on the sheath of active filamentous and coccoid cyanobacteria, and very little carbonate precipitation occurs where photosynthesis peaks (in the mat subsurface).
3 *As a result of (1) and (2), no significant precipitation of carbonate results from CO_2 uptake by cyanobacteria.
4 The non-lithifying mat in Salt Pan sustains lower microbial metabolic rates than the lithifying mat and does not have a clear peak in SRB activity.
5 In thin sections, precipitates often have a micritic micropeloidal microstructure surrounded by microspar and spar cements. Micritic micropeloids exhibit higher fluorescence than the surrounding microspar and spar cement.
6 Precipitation occurs within the alveolar structure of EPS matrix and progressively fills the space in between bacteria.
7 *Favourable conditions for carbonate precipitation in microenvironments can be created by the decoupling of microbial metabolism in time and space. When the activity of SRB is high, net carbonate precipitation results.
8 *Initially, acidic macromolecules in the EPS biofilm inhibit carbonate precipitation, resulting in non-calcifying mats in the middle of the lake. Precipitation is induced when Ca^{2+} availability exceeds the binding capacity of the EPS and/or binding capacity is reduced through decarboxylation, which occurs at shallower depths. The initial microstructure of the precipitate consists of 200–500 nm spheres that develop rounded

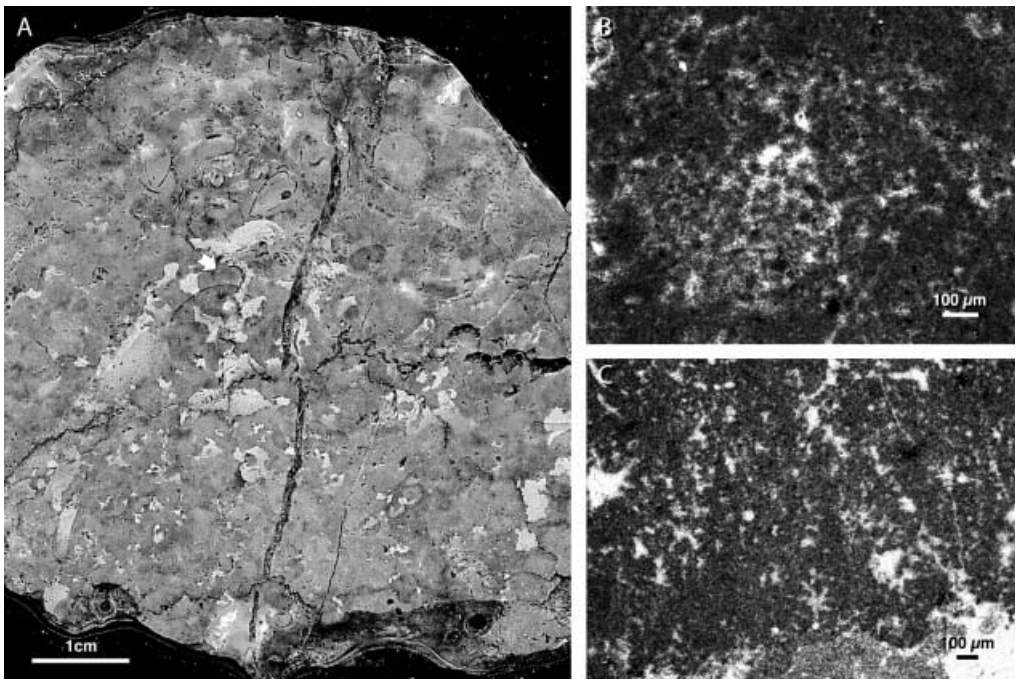

Fig. 12. Example of Jurassic thrombolite. (A) Thrombolite mesostructure showing mesoclots (white arrows) surrounded by dolomitized allochthonous micrite (black arrows). This mesostructure represents the typical 'clotted' fabric of the thrombolite. Sample HR21, polished slab. (B) and (C) Mesoclot microstructure made of micropeloids surrounded by microspar and spar cement. Sample HR21, thin sections.

crystal shapes. This may result from: (a) a process similar to high-Mg calcite precipitation in an acidic EPS matrix (Braissant *et al.*, 2003); (b) random and scattered precipitation resulting from highly organized macromolecules, which bind cations and provide hotspots of calcium precipitation on an organic template; (c) the entombment of small bacteria.

9 *Degradation of EPS by fermentation or UV light leads to hydrolysis or decarboxylation of EPS and the formation of lmw organic compounds that support SRB. Hydrolysis and decarboxylation of EPS liberates cations and results in an internal increase in $[Ca^{2+}]$ and $[Mg^{2+}]$. Sulphate reduction then increases alkalinity in microdomains inside the EPS. With abundant $[Ca^{2+}]$ and $[Mg^{2+}]$ available, this leads to calcification of EPS.

10 *The decrease in pH resulting from CO_2 produced during decarboxylation is buffered by alkaline water from Salt Pan.

11 *The initial product is discontinuously calcified EPS, which forms 'fuzzy-edged' micropeloids of micrite visible with light microscopy, with an intense autofluorescence resulting from high organic content. Subsequently, alkalinity of Salt Pan promotes physico-chemical precipitation of microsparite and sparite on the EPS-free substrate (micropeloids). This results in the formation of fuzzy micropeloids surrounded by microspar.

Further investigations are needed to test this conceptual model. EPS need to be characterized because of the variety of chemical and microbiological factors that can affect the composition and ability to precipitate carbonate. In addition, the current work attempts to characterize the microbial community composition in a better way. The use of fluorescent *in situ* hybridization (FISH; Amann & Kühl, 1998) will enable precise localization of the SRB detected through silver foil measurement. Future work will also include a long-term hydrochemical survey in order to understand better seasonal fluctuations in microbialite formation and preservation.

ACKNOWLEDGEMENTS

We are grateful to Massoud Dadras and Mireille Leboeuf for their availability and helpful advice using low-temperature SEM, Don A. Dean (Smithsonian Institution) for making the petrographic thin sections, Dr Thierry Adatte for performing the X-ray analyses, Olivier Braissant and Guillaume Cailleau for valuable discussions and help with the sample preparation (X-ray). The crew of the R/V *Walton Smith* are thanked for their assistance. This work was supported by the US National Science Foundation Biogeosciences program (grant no. NSF 0311929). The first author is grateful to the Swiss National Science Foundation for its support through the 'Fellowship for Prospective Researchers'. We wish to thank associate editor, Dr Christoph Spötl, Dr Robert Riding and an anonymous reviewer for their thoughtful remarks on the manuscript and their suggestions for future work. This paper is Research Initiative on Bahamian Stromatolites (RIBS) contribution 24.

REFERENCES

Addadi, L. and **Weiner, S.** (1989) Stereochemical and structural relations between macromolecules and crystals in biomineralisation. In: *Biomineralization* (Eds S. Mann, J. Webb and R.J.P. Williams), pp. 133–156. VCH, Weinheim.

Aitken, J.D. (1967) Classification and environmental significance of cryptalgal limestones and dolomites, with illustrations from the Cambrian and Ordovician of southwestern Alberta. *J. Sed. Petrol.*, **37,** 1163–1178.

Amman, R. and **Kühl, M.** (1998) In situ methods for the assessment of organisms and their activities. *Curr. Opin. Microbiol.*, **1,** 352–358.

Arp, G., Hofmann, J. and **Reitner, J.** (1998) Microbial fabric formation in spring mounds ('Microbialites') of alkaline Salt Lakes in the Badain Jaran Sand Sea, PR China. *Palaios*, **13,** 581–592.

Arp, G., Reimer, A. and **Reitner, J.** (1999a) Calcification in cyanobacterial biofilms of alkaline salt lakes. *Eur. J. Phycol.*, **34,** 393–403.

Arp, G., Thiel, V., Reimer, A., Michaelis, W. and **Reitner, J.** (1999b) Biofilm exopolymers control microbialite formation at thermal springs discharging into the alkaline Pyramid Lake, Nevada, USA. *Sed. Geol.*, **126,** 159–176.

Arp, G., Reimer, A. and **Reitner, J.** (2001) Photosynthesis-induced biofilm calcification and calcium concentrations in Phanerozoic oceans. *Science*, **292,** 1701–1704.

Arp, G., Reimer, A. and **Reitner, J.** (2003) Microbialite formation in seawater of increased alkalinity, Satonda Crater Lake, Indonesia. *J. Sed. Res.*, **73,** 105–127.

Bosence, D.W.J. and **Bridges, P.H.** (1995) A review of the origin and evolution of carbonate mud-mounds. *IAS Spec. Publ.*, **23,** 3–9.

Brading, M.G., Jass, J. and **Lappin-Scott, H.M.** (1995) Dynamics of bacterial biofilm formation. In: *Microbial Biofilms* (Eds H.M. Lappin-Scott and J.W. Costerton), pp. 46–63. Cambridge University Press, Cambridge.

Braissant, O., Cailleau, G., Dupraz, C. and **Verrecchia, E.P.** (2003) Bacterially induced mineralization of calcium carbonate in terrestrial environments: the role of exopolysaccharides and amino acids. *J. Sed. Res.*, **73,** 483–488.

Canfield, D.E. and **Des Marais, D.J.** (1991) Aerobic sulfate reduction in microbial mats. *Science*, **251,** 1471–1473.

Canfield, D.E. and **Des Marais, D.J.** (1993) Biogeochemical cycles of carbon, sulfur, and free oxygen in a microbial mat. *Geochim. Cosmochim. Acta*, **57,** 3971–3984.

Canfield, D.E. and **Des Marais, D.J.** (1994) Cycling of carbon, sulfur, oxygen and nutrients in a microbial mat. In: *Microbial Mats: Structure, Development and Environmental Significance* (Eds L.J. Stal and P. Caumette), pp. 255–263. Springer-Verlag, Berlin.

Castanier, S., Maurin, A. and **Perthuisot, J.-P.** (1989) Production bactérienne expérimentale de corpuscules carbonates, sphéroïdaux à structure fibroradiaire. *Bull. Soc. Géol. Fr.*, **8,** 589–595.

Chafetz, H.S. (1986) Marine peloids: a product of bacterially induced precipitation of calcite. *J. Sed. Petrol.*, **56,** 812–817.

Costerton, J.W., Lewandowski, Z., Caldwell, D.E., Korber, D.R. and **Lappin-Scott, H.M.** (1995) Microbial biofilms. *Annu. Rev. Microbiol.*, **49,** 711–745.

Decho, A.W. (1990) Microbial exopolymer secretions in ocean environments: their role(s) in food webs and marine processes. *Oceanogr. Mar. Biol. Annu. Rev.*, **28,** 73–154.

Decho, A.W. (2000) Exopolymer microdomains as a structuring agent for heterogeneity within microbial biofilms. In: *Microbial Sediments* (Eds R.E. Riding and S.M. Awramik), pp. 1–9. Springer-Verlag, Berlin.

Défarge, C., Tribble, J., Sansone, F.J., Trichet, J., Jaunet, A.-M. and **Robert, M.** (1996) Texture of microbial sediments revealed by cryo-scanning electron microscopy. *J. Sed. Res.*, **66,** 935–947.

Des Marais, D.J. (1997) Long-term evolution of the biogeochemical carbon cycle. In: *Geomicrobiology, Interactions between Microbes and Minerals* (Eds J.E. Banfield, and K.H. Nealson), pp. 427–448. Mineral. Soc. Am., Washington, DC.

Dupraz, C. and **Strasser, A.** (1999) Microbialites and microencrusters in shallow coral bioherms (Middle to Late Oxfordian, Swiss Jura Mountains). *Facies*, **40,** 101–130.

Dupraz, C. and **Strasser, A.** (2002) Nutritional modes in coral–microbialite reefs (Jurassic, Oxfordian, Switzerland): evolution of trophic structure as a response to environmental change. *Palaios*, **17,** 449–471.

Epping, E.H.G., Khalili, A. and **Thar, R.** (1999) Photosynthesis and the dynamics of oxygen consumption in a microbial mat as calculated from transient oxygen microprofiles. *Limnol. Oceanogr.*, **44,** 1936–1948.

Ferris, F.G., Schultze, S., Witten, T.C., Fyfe, W.S. and **Beveridge, T.J.** (1989) Metal interactions with microbial biofilms in acidic and neutral pH environments. *Appl. Environ. Microbiol.*, **55,** 1249–1257.

Folk, R.L. (1959) Practical petrographic classification of limestones. *Bull. AAPG*, **43,** 1–38.

Folk, R.L. and **Chafetz, H.S.** (2000) Bacterially induced microscale and nanoscale carbonate precipitates. In: *Microbial Sediments* (Eds R.E. Riding and S.M. Awramik), pp. 40–49. Springer-Verlag, Berlin.

Freytet, P. and **Verrecchia, E.P.** (1998) Freshwater organisms that build stromatolites: a synopsis of biocrystallization by prokaryotic and eukaryotic algae. *Sedimentology*, **45,** 535–563.

Freytet, P. and **Verrecchia, E.P.** (2002) Lacustrine and palustrine carbonate petrography: an overview. *J. Paleolimnol.*, **27,** 221–237.

Fründ, C. and **Cohen, Y.** (1992) Diurnal cycles of sulfate reduction under oxic conditions in cyanobacterial mats. *Appl. Environ. Microbiol.*, **58,** 70–77.

Hillgärtner, H., Dupraz, C. and **Hug, W.A.** (2001) Microbially induced stabilization of carbonate sands in marine phreatic environments or are micritic meniscus cements good indicators for vadose diagenesis? *Sedimentology*, **48,** 117–132.

Kennard, J.M. and **James, N.P.** (1986) Thrombolites and stromatolites: two distinct types of microbial structures. *Palaios*, **1,** 492–503.

Kirkland, B.L., Lynch, F.L., Rahnis, M.A., Folk, R.L., Molineux, I.J. and **McLean, R.J.C.** (1999) Alternative origins for nanobacteria-like objects in calcite. *Geology*, **27,** 347–350.

Knoll, A. (1999) Over*view. Size Limits of Very Small Microorganisms (Proceeding), Space Studies Board and National Research Council*, pp. 1–5. National Academy Press, Washington, DC.

Krumbein, W.E. (1983) Stromatolites – the challenge of a term in space and time. *Precambrian Res.*, **20,** 493–531.

Krumbein, W.E. and **Swart, P.K.** (1983) The microbial carbon cycle. In: *Microbial Geochemistry* (Ed. W.E. Krumbein), pp. 5–62. Blackwell, Oxford.

Krumbein, W.E., Paterson, D.M. and **Zavarzin, G.A.** (2003) *Fossil and Recent Biofilms: A Natural History of the Impact of Life on Planet Earth.* Kluwer Scientific Publishers, Dordrecht, The Netherlands, 482 pp.

Kübler, B. (1992) Calcites magnésiennes: identification et dosage par diffraction X de $MgCO_3$ dans la solution solide. *Cah. Inst. Géol. Lab. Minéral. Pétrogr. Géochim., Univ. Neuchâtel, Série AX*, **N22,** 1–15.

Laurenti, A. and **Montaggioni, L.** (1995) Importance de l'activité microbienne dans la lithification marine récifale (Tahiti, Polynésie française). *Acad. Sci. Paris*, **320,** 845–852.

Leinfelder, R.R., Werner, W., Nose, M., Schmid, D.U., Krautter, M., Laternser, R., Takacs, M. and **Hartmann, D.** (1996) Paleoecology, growth parameters and dynamics of coral, sponge and microbialite reefs from the Late Jurassic. In: *Global and Regional Controls on Biogenic Sedimentation. I. Reef Evolution. Research Reports* (Eds J. Reitner, F. Neuweiler and F. Gunkel), *Göttinger Arb. Geol. Paläont*, **Sb2,** 227–248.

Little, B.J., Wagner, P.A. and **Lewandowski, Z.** (1997) Spatial relationships between bacteria and mineral surfaces. In: *Geomicrobiology, Interactions between Microbes and Minerals* (Ed. P.H. Ribbe), *Rev. Mineral.*, **35,** 123–159.

McConnaughey, T.A. and **Whelan, J.F.** (1997) Calcification generates protons for nutrient and bicarbonate uptake. *Earth Sci. Rev.*, **42,** 95–117.

Merz-Preiß, M. and **Riding, R.** (1999) Cyanobacterial tufa calcification in two freshwater streams: ambient environment, chemical thresholds and biological processes. *Sed. Geol.*, **126,** 103–124.

Nealson, K.H. and **Ghiorse, W.A.** (2001) *Geobiology: Exploring the Interface between the Biosphere and the Geosphere.* American Academy of Microbiology, Washington, DC, 17 pp.

Nealson, K.H. and **Stahl, D.A.** (1997) Microorganisms and biogeochemical cycles: what can we learn from layered microbial communities? In: *Geomicrobiology, Interactions between Microbes and Minerals* (Eds J.F. Banfield and K.H. Nealson), *Mineral. Soc. Am. Rev. Mineral.*, **35,** 5–34.

Neuweiler, F., Gautret, P., Volker, T., Langes, R., Michaelis, W. and **Reitner, J.** (1999) Petrology of Lower Cretaceous carbonate mud mounds (Albian, N. Spain): insights into organomineralic deposits of the geological record. *Sedimentology*, **46,** 837–859.

Neuweiler, F., Rutsch, M., Geipel, G., Reimer, A. and **Heise, K.-H.** (2000) Soluble humic substances from in situ precipitated microcrystalline calcium carbonate, internal

sediment, and spar cement in a Cretaceous carbonate mudmound. *Geology*, **28,** 851–854.

Olavi Kajander, E., Björklund, M. and **Çiftçioglu, N.** (1999) Suggestion from observations on nanobacteria isolated from blood. In: *Size Limits of Very Small Microorganisms (Proceeding), Space Studies Board and National Research Council*, pp. 50–55. National Academy Press, Washington, DC.

Pentecost, A. (1985) Association of cyanobacteria with tufa deposits: identity, enumeration and nature of the sheath material revealed by histochemistry. *Geomicrobiology*, **4,** 285–298.

Reid, R.P., Visscher, P.T., Decho, A.W., Stolz, J.K., Bebout, B.M., Dupraz, C., Macintyre, I.G., Paerl, H.W., Pinckney, J.L., Prufert-Bebout, L., Steppe, T.F. and **DesMarais, D.J.** (2000) The role of microbes in accretion, lamination and early lithification of modern marine stromatolites. *Nature*, **406,** 989–992.

Reid, R.P., Dupraz, C., Visscher, P.T., Decho, A.W. and **Sumner, D.Y.** (2003) Microbial processes forming modern marine stromatolites: microbe–mineral interactions with a three-billion-year rock record. In: *Fossil and Recent Biofilms – a Natural History of Life on Earth* (Eds W.E. Krumbein, D.M. Paterson and G.A. Zavarzin), pp. 103–118. Kluwer Academic Publishers, Dordrecht, The Netherlands.

Reitner, J. (1993) Modern cryptic microbialite/metazoan facies from Lizard Island (Great Barrier Reef, Australia) formation and concepts. *Facies*, **29,** 2–40.

Reitner, J., Gautret, P., Marin, F. and **Neuweiler, F.** (1995) Automicrites in modern marine microbialite. Formation model via organic matrices (Lizard Island, Great Barrier Reef, Australia). *Bull. Inst Océanogr. Monaco Spec. No.*, **14,** 237–264.

Reitner, J., Arp, G., Thiel, V., Gautret, P., Galling, U. and **Michaelis, W.** (1997) Organic matter in Great Salt Lake ooids (Utah, USA): first approach to a formation via organic matrices. *Facies*, **36,** 210–219.

Riding, R. (1991) Classification of microbial carbonates. In: *Calcareous Algae and Stromatolites* (Ed. R. Riding), pp. 21–51. Springer-Verlag, New York.

Riding, R. (2000) Microbial carbonates: the geological record of calcified bacterial-algal mats and biofilms. *Sedimentology*, **47,** 179–214.

Riding, R. (2002) Structure and composition of organic reefs and carbonate mud mounds: concepts and categories. *Earth-Sci. Rev.*, **58,** 163–231.

Robbins, L.L. and **Blackwelder, P.L.** (1992) Biochemical and ultrastructural evidence for the origin of whitings: a biologically induced calcium carbonate precipitation mechanism. *Geology*, **20,** 464–468.

Schieber, J. and **Arnott, H.J.** (2003) Nanobacteria as a by-product of enzyme-driven tissue decay. *Geology*, **31,** 717–720.

Shapiro, R.S. (2000) A comment on the systematic confusion of thrombolites. *Palaios*, **15,** 166–169.

Stal, L.J., van Gemerden, H. and **Krumbein, W.E.** (1985) Structure and development of a benthic marine microbial mat. *FEMS Microbiol. Ecol.*, **31,** 111–125.

Thompson, J.B., Schultze-Lam, S., Beveridge, J. and **Des Marais, D.J.** (1997) Whiting events: biogenic origin due to the photosynthetic activity of cyanobacterial picoplankton. *Limnol. Oceanogr.*, **42,** 133–141.

Trichet, J. and **Défarge, C.** (1995) Non-biologically supported organomineralization. *Bull. Inst. Océanogr. Monaco Spec. No.*, **14,** 203–236.

Trichet, J., Défarge, C., Tribble, J., Tribble, G. and **Sansone, F.** (2001) Christmas Islands lagoonal lakes, models for the deposition of carbonate-evaporite-organic laminated sediments. *Sed. Geol.*, **140,** 177–189.

Uhlinger, D.J. and **White, D.C.** (1983) Relationship between physiological status and formation of extracellular polysaccharide glycocalyx in *Pseudomonas altantica*. *Appl. Environ. Microbiol.*, **45,** 64–70.

Van Gemerden, H. (1993) Microbial mats: a joint venture. *Mar. Geol.*, **113,** 3–25.

Van Lith, Y. (2001) *The role of sulphate-reducing bacteria in dolomite formation: a study of a Recent environment, bacterial cultures, and dolomite concretions*. PhD Thesis, Geological Institute, Swiss Federal Institute of Technology, ETH, Zürich, Switzerland.

Van Lith, Y., Warthmann, R., Vasconcelos, C. and **McKenzie, J.A.** (2003) Microbial fossilization in carbonate sediments: a result of the bacterial surface involvement in dolomite precipitation. *Sedimentology*, **50,** 237–245.

Verrecchia, E.P., Freytet, P., Verrecchia, K.E. and **Dumont, J.L.** (1995) Spherulites in calcrete laminar crusts: biogenic CaCO3, precipitation as a major contributor to crust formation. *J. Sed. Res.*, **A65,** 690–700.

Visscher, P.T., Beukema, J. and **van Germerden, H.** (1991) *In situ* characterization of sediments: Measurements of oxygen and sulfide profiles with a novel combined needle electrode. *Limnol. Oceanogr.*, **36,** 1476–1480.

Visscher, P.T., Prins, R.A. and **van Gemerden, H.** (1992a) Rates of sulfate reduction and thiosulfate consumption in a marine microbial mat. *FEMS Microbiol. Ecol.*, **86,** 283–294.

Visscher, P.T., van den Ende, F.P., Schaub, B.E.M. and **van Gemerden, H.** (1992b) Competition between anoxygenic phototrophic bacteria and colorless sulfur bacteria in a microbial mat. *FEMS Microbiol. Ecol.*, **101,** 51–58.

Visscher, P.T., Reid, R.P., Debout, B.M., Hoeft, S.E., Macintyre, I.G. and **Thompson, J.A., Jr** (1998) Formation of lithified micritic laminae in modern marine stromatolites (Bahamas): the role of sulfur cycling. *Am. Mineral.*, **83,** 1482–1491.

Visscher, P.T., Reid, R.P. and **Bebout, B.M.** (2000) Microscale observations of sulfate reduction: correlation of microbial activity with lithified micritic laminae in modern marine stromatolites. *Geology*, **28,** 919–922.

Visscher, P.T., Surgeon, T.M., Hoeft, S.E., Bebout, B.M., Thompson, J.,Jr and **Reid, R.P.** (2002) Microelectrode studies in modern marine stromatolites: unraveling the Earth's past? In: *Electrochemical Methods for the Environmental Analysis of Trace Metal Biogeochemistry* (Eds M. Taillefert and T. Rozan), pp. 265–282. ACS Symposium Series 220. Cambridge University Press, New York.

Manuscript received 3 April 2003;
revision accepted 28 January 2004.